Numerical method for coherent electron dynamics with position-dependent effective-mass distributions in semiconductor heterostructures

Taro Ando* and Yoshiyuki Ohtake
The 1st Research Group, Central Research Laboratory, Hamamatsu Photonics K. K., 5000 Hirakuchi, Hamamatsu-City, Shizuoka, 434-8601, Japan

Naoki Ohtani
Department of Electronics, Faculty of Engineering, Doshisya University, 1-3 Tataramiyakodani, Kyotanabe-City, Kyoto, 610-0321, Japan

(Received 26 December 2005; published 5 June 2006)

We develop a numerical scheme for solving the time-dependent Kohn-Sham equation in semiconductor heterostructures. Based on the efficient and accurate method recently proposed by Watanabe and Tsukada [Phys. Rev. E **65**, 036705 (2002)], an extension is made for treating effective-mass mismatch between different semiconductor materials. A demonstrative calculation shows that the energy of the quantum-well state is accurately conserved during the time-evolution calculation with the present method. Examples under the existence of Hartree and exchange-correlation interactions are also shown as demonstrations of nonlinear electron dynamics in quantum wells. The present method is particularly useful for analyzing nonlinear coherent charge oscillations in semiconductor quantum wells, taking into account many-body effects.

DOI: 10.1103/PhysRevE.73.066702 PACS number(s): 02.70.−c, 71.15.Qe, 71.15.Mb, 73.21.−b

I. INTRODUCTION

The effective-mass Kohn-Sham (KS) equation has been used for examining the quantum states of semiconductor heterostructures, e.g., accumulation or inversion layers [1], quantum wells (QWs) [2–6], and superlattices [7], taking many-body effects of carriers into account. Thus, analogous to the time-dependent KS (TDKS) equation commonly applied to the *ab initio* calculation of dynamical phenomena and excited states in various materials [8], we can expect the effective-mass TDKS equation to be also effective for the coherent charge dynamics and excited states in QWs. However, there are no reports to date on the study of quantum states with the TDKS equation involving the effective-mass mismatch, which causes significant effects in real semiconductor heterostructures [9–11].

Although straightforward implementation of the effective-mass mismatch is itself possible based on the usual integration methods, such methods do not practically work for time-evolution calculations over long time periods: simple methods such as the Newton-Raphson method and the Runge-Kutta method can perform calculations efficiently but fail due to accumulation of numerical errors [12], while accurate methods such as the Clank-Nicholson method and the alternating directional implicit method can derive accurate results but require much computational time. Thus it is necessary to develop a numerical method that can solve the effective-mass TDKS accurately and efficiently even in the existence of the effective-mass mismatch. In this paper, we develop an efficient and stable scheme for solving the TDKS equation with position-dependent effective-mass distribution that is based upon the method proposed by Watanabe and Tsukada [12]. The essence of the present method is to solve the effective-mass TDKS equation on discretized space with the help of exponential-product expansion. In order to treat the spatial distribution of the electron effective mass, we extend the space-splitting procedure [13–15], in which a discretized Laplacian is decomposed into two block-diagonal matrices, to treat the kinetic-energy operator involving a position-dependent mass. Resultantly, the present method can evaluate accurate results even for time evolutions over very long time periods, following which the method is suitable for analyzing subband structures of small energy differences.

Usually, the semiconductor Bloch equation is widely applied for studying the temporal response of carriers in semiconductors [16]. However, foreknowledge of the energy level structure and of transition matrix elements is required to construct the Bloch equation, while the present method automatically provides time-evolution results once the band structure and initial state are defined. Thus, the present method can be applied flexibly to systems of complex structure and is suitable for analyzing coherent charge dynamics in semiconductor heterostructures with many-body interactions, and above all, dynamical response to a slowly oscillating electric field, whose energy is sufficiently smaller than that required for interband transition.

II. FORMULATION

In this section, we define a TDKS equation with position-dependent effective mass and establish formulations for solving the equation. The effective-mass TDKS equation is applicable to general semiconductor heterostructures such as quantum wires and dots, though for simplicity the formulation is restricted to a QW system in this paper.

*Electronic address: taro@crl.hpk.co.jp

When electrons are confined in one-dimensional semiconductor heterostructures (growth direction z), time evolution of the one-electron wave function ψ_n is described with the following TDKS equation in a mean-field approach:

$$i\hbar\frac{\partial}{\partial t}\psi_n(z,t) = \mathcal{H}[\rho;z,t]\psi_n(z,t),$$

$$\mathcal{H}[\rho;z,t] = \hat{K}(z) + \hat{V}[\rho;z,t]. \tag{1}$$

In the density functional theory (DFT) [17], the electron density ρ is usually defined as the following:

$$\rho(z,t) = \sum_{n=1}^{N_0} |\psi_n(z,t)|^2, \tag{2}$$

where N_0 is the total number of electrons in the system and n is the index of each quantum state occupied with the electron. The effective potential ($\hat{V}[\rho;z,t]$) is given as a sum of two parts: one is an internal mutual interaction component $\hat{V}_{\text{int}}[\rho;z]$, which is a functional of ρ and dependent on the time implicitly via ρ, while the other is an external potential component $\hat{V}_{\text{ext}}(z,t)$, which depends explicitly on the time and position but not on ρ. Although the band-edge potential is not a function of the time, it is treated as a component of the external potential in our formulation. Explicit expressions of the interaction terms will be given later.

A significant difference of the present effective-mass TDKS equation [Eq. (1)] from ordinal TDKS equation is the following "variable-mass" kinetic-energy operator [11]:

$$\hat{K}(z) = -\frac{\hbar^2}{2}\frac{\partial}{\partial z}\frac{1}{m(z)}\frac{\partial}{\partial z}, \tag{3}$$

where $m(z)$ denotes the position-dependent effective mass of an electron. It should be stressed that $\hat{K}$ is a Hermitian operator.

In general, the formal solution of Eq. (1) is given as the following with a time-ordering operator T:

$$\psi_n(z,t) = T\exp\left(\frac{1}{i\hbar}\int_0^t dt'\mathcal{H}[\rho;t']\right)\psi_n(z,0). \tag{4}$$

Watanabe's method gives a practical procedure for calculating Eq. (4). To clarify the modification included in this paper, we briefly outline the formulation of Ref. [12] in the following. Applying a Taylor development in exponential form and the chain rule of the derivative, a short-time evolution of a wave function is written as

$$\psi_n(z,t+\Delta t) = \exp\left[\frac{\Delta t}{i\hbar}\left((\mathcal{H}[\rho;z,t]\psi)\frac{\delta}{\delta\psi} - (\mathcal{H}[\rho;z,t]\psi)^*\frac{\delta}{\delta\psi^*} + i\hbar\frac{\partial}{\partial t_{\text{ex}}}\right)\right]\psi_n(z,t), \tag{5}$$

where $\partial/\partial t_{\text{ex}}$ is an explicit time-derivative operator. Here we note that the following notation for a general functional $f[\{\psi\},\{\psi^*\},t]$ in Ref. [12] has been applied:

$$(\mathcal{H}\psi)\frac{\delta f}{\delta\psi} \equiv \sum_{n=1}^{N_0}\int dz[\mathcal{H}\psi_n(z)]\frac{\partial f}{\partial\psi_n(z)}. \tag{6}$$

With the help of the exponential-operator expansion [18], Eq. (5) is written as

$$\begin{aligned}\psi_n(z,t+\Delta t) &= \exp\left(\frac{\Delta t}{2}\frac{\partial}{\partial t_{\text{ex}}}\right)\exp\left[\frac{\Delta t}{2}\frac{1}{i\hbar}\left((\hat{K}\psi)\frac{\delta}{\delta\psi} - (\hat{K}\psi)^*\frac{\delta}{\delta\psi^*}\right)\right]\\ &\times\exp\left[\frac{\Delta t}{i\hbar}\left((\hat{V}[\rho;z,t]\psi)\frac{\delta}{\delta\psi} - (\hat{V}[\rho;z,t]\psi)^*\frac{\delta}{\delta\psi^*}\right)\right]\\ &\times\exp\left[\frac{\Delta t}{2}\frac{1}{i\hbar}\left((\hat{K}\psi)\frac{\delta}{\delta\psi} - (\hat{K}\psi)^*\frac{\delta}{\delta\psi^*}\right)\right]\\ &\times\exp\left(\frac{\Delta t}{2}\frac{\partial}{\partial t_{\text{ex}}}\right)\psi_n(z,t) + O(\Delta t^2).\end{aligned} \tag{7}$$

Among exponentials on the right-hand side (RHS) of Eq. (7), the exponential of $\hat{V}$ can be treated in the same way as in Ref. [12]. Thus, care is needed only for the kinetic-energy operator.

In Ref. [12], the exponential of Laplacian Δ was evaluated using a Taylor series expansion, and higher-order terms of the Taylor series were evaluated inductively from the first-order relation, i.e.,

$$\left[(\Delta\psi)\frac{\delta}{\delta\psi} - (\Delta\psi)^*\frac{\delta}{\delta\psi^*}\right]\psi_n = \Delta\psi_n. \tag{8}$$

Here, it is obvious that Eq. (8) is still correct even if Δ is replaced with $\hat{K}$, because $\hat{K}$ does not depend on ψ nor ψ^*. From the higher-order relations (see the Appendix), we obtain the following equation for the exponential of $\hat{K}$:

$$\begin{aligned}&\exp\left[\frac{\Delta t}{2}\frac{1}{i\hbar}\left((\hat{K}\psi)\frac{\delta}{\delta\psi} - (\hat{K}\psi)^*\frac{\delta}{\delta\psi^*}\right)\right]\psi_n(z,t)\\ &= \exp\left(\frac{\Delta t}{2}\frac{\hat{K}}{i\hbar}\right)\psi_n(z,t).\end{aligned} \tag{9}$$

Thus, the formula for short-time evolution becomes

$$\begin{aligned}\psi_n(z,t+\Delta t) &= \exp\left(\frac{\Delta t}{2}\frac{\hat{K}}{i\hbar}\right)\\ &\times\exp\left\{\frac{\Delta t}{i\hbar}\left[\hat{V}_{\text{int}}[\rho';z] + \hat{V}_{\text{ext}}\left(z,t+\frac{\Delta t}{2}\right)\right]\right\}\\ &\times\exp\left(\frac{\Delta t}{2}\frac{\hat{K}}{i\hbar}\right)\psi_n(z,t) + O(\Delta t^2),\end{aligned} \tag{10}$$

where ρ' is given as

$$\rho'(z,t) = \sum_{n=1}^{N_0}\left|\exp\left(\frac{\Delta t}{2}\frac{\hat{K}}{i\hbar}\right)\psi_n(z,t)\right|^2. \tag{11}$$

The above equations indicate that Watanabe's formulation is valid also for the variable-mass kinetic-energy operator, i.e., $\hat{K}$.

In the present method, the kinetic-energy operator is further decomposed into a sum of two parts, whose exponentials can be easily calculated, i.e., $\hat{K}=\hat{K}_e+\hat{K}_o$ (explicit expressions are given in Sec. III). Applying the second-order exponential-operator expansion, exponentials of $\hat{K}$ in Eqs. (10) and (11) are replaced with

$$\exp\left(\frac{\Delta t}{2}\frac{\hat{K}}{i\hbar}\right) \approx \exp\left(\frac{\Delta t}{4}\frac{\hat{K}_e}{i\hbar}\right)\exp\left(\frac{\Delta t}{2}\frac{\hat{K}_o}{i\hbar}\right)\exp\left(\frac{\Delta t}{4}\frac{\hat{K}_e}{i\hbar}\right). \tag{12}$$

It should be noted that the above expansion is correct up to the order of $O(\Delta t^2)$ and thus the time-dependent nature of the density in Ref. [12], i.e.,

$$\rho' = \rho\left(t+\frac{\Delta t}{2}\right) + O(\Delta t^2), \tag{13}$$

is also valid. Therefore, by substituting Eq. (12) into Eqs. (10) and (11), Eq. (10) is rewritten as

$$\psi_n(z,t+\Delta t) = S_2(\Delta t;t)\psi_n(z,t), \tag{14}$$

where

$$S_2(\Delta t;t) = \exp\left(\frac{\Delta t}{4}\frac{\hat{K}_e}{i\hbar}\right)\exp\left(\frac{\Delta t}{2}\frac{\hat{K}_o}{i\hbar}\right)\exp\left(\frac{\Delta t}{4}\frac{\hat{K}_e}{i\hbar}\right) \times \exp\left\{\frac{\Delta t}{i\hbar}\left[\hat{V}_{\mathrm{int}}[\rho';z]+\hat{V}_{\mathrm{ext}}\left(z,t+\frac{\Delta t}{2}\right)\right]\right\} \times \exp\left(\frac{\Delta t}{4}\frac{\hat{K}_e}{i\hbar}\right)\exp\left(\frac{\Delta t}{2}\frac{\hat{K}_o}{i\hbar}\right)\exp\left(\frac{\Delta t}{4}\frac{\hat{K}_e}{i\hbar}\right). \tag{15}$$

$S_2(\Delta t;t)$ gives a symmetric decomposition of the total time-evolution operator that is accurate up to the second order of Δt. Formulas of higher-order accuracy are also derived using $S_2(\Delta t;t)$, according to the property of exponential-product expansion [18].

III. NUMERICAL PROCEDURE

In this section, we describe numerical expressions for practical calculations on the discretized space. Here, one-dimensional space (z) is discretized into a finite mesh with equal interval Δz, and each point is labeled by an integer $j=1,2,\ldots,N$, where N is assumed to be an even integer. According to the discretization, a wave function is expressed as a N-dimensional vector, whereas an operator generally becomes an $N\times N$ matrix that acts on the discretized wave function.

To derive a matrix representation of the time-evolution operator [Eq. (15)], exponentials of $\hat{K}_e$, $\hat{K}_o$, and $\hat{V}$ must be given on the discretized space. In the following, we define the explicit expressions of $\hat{K}_e$ and $\hat{K}_o$ and calculate exponentials of them. From Eq. (3), $\hat{K}$ is given as follows on the discretized space:

$$K = \frac{\hbar^2}{2(\Delta z)^2}\begin{pmatrix} \left(\frac{1}{m_1^-}+\frac{1}{m_1^+}\right) & -\frac{1}{m_1^+} & 0 & \cdots & 0 \\ -\frac{1}{m_2^-} & \left(\frac{1}{m_2^-}+\frac{1}{m_2^+}\right) & -\frac{1}{m_2^+} & 0 & \vdots \\ 0 & -\frac{1}{m_3^-} & \ddots & \ddots & 0 \\ \vdots & 0 & \ddots & \ddots & -\frac{1}{m_{N-1}^+} \\ 0 & \cdots & 0 & -\frac{1}{m_N^-} & \left(\frac{1}{m_N^-}+\frac{1}{m_N^+}\right) \end{pmatrix}, \tag{16}$$

where each $m_i^{\pm}$ is defined as

$$m_i^{\pm} = (m_i + m_{i\pm1})/2, \quad m_1^- = m_1, \quad m_N^+ = m_N, \tag{17}$$

with a discretized effective-mass distribution m_i [19]. Equation (17) leads to $m_i^+ = m_{i+1}^-$, indicating that the matrix defined in Eq. (16) is a real symmetrical matrix, i.e., a matrix representation of an Hermitian operator.

An exponential of K cannot, however, be expressed in a suitable form for practical calculations. To obtain an expression convenient for numerical computations, the matrix K is split into "even" and "odd" parts ($K=K_e+K_o$), both of whose

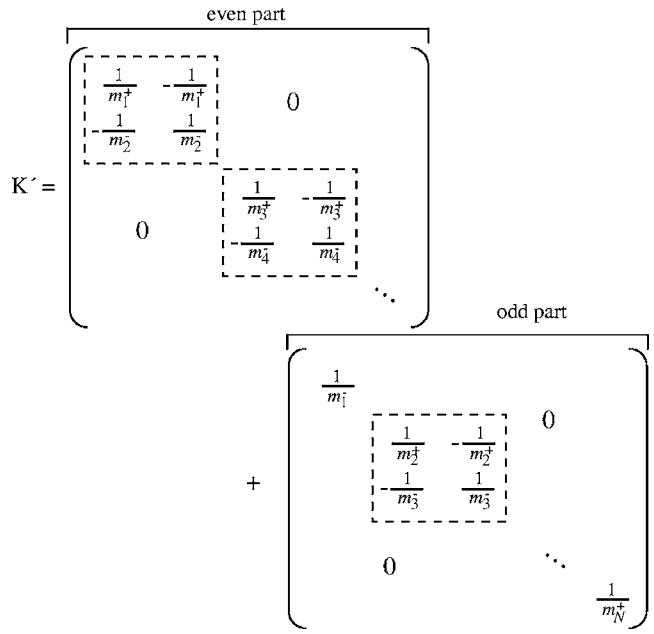

FIG. 1. Schematic diagram of the space-splitting procedure applied to the kinetic-energy part of the Hamiltonian $[K' = (2\Delta z^2/\hbar^2)K]$. We note that absolute values of the four elements become equal [see Eq. (17)] in each 2×2 block matrix surrounded with a dashed square.

exponentials are expressed analytically [13–15]. Figure 1 shows a schematic diagram of the space-splitting procedure. According to the space splitting, K_e and K_o become block-diagonal matrices:

$$\alpha K_e = \frac{M}{m_1^+} \oplus \frac{M}{m_3^+} \oplus \cdots \oplus \frac{M}{m_{N-1}^+}, \tag{18}$$

$$\alpha K_o = \frac{1}{m_1^-} \oplus \frac{M}{m_2^+} \oplus \frac{M}{m_4^+} \oplus \cdots \oplus \frac{M}{m_{N-2}^+} \oplus \frac{1}{m_N^+}, \tag{19}$$

respectively, with

$$M = \begin{pmatrix} 1 & -1 \\ -1 & 1 \end{pmatrix} \tag{20}$$

and $\alpha = 2(\Delta z)^2/\hbar^2$. Considering the fact that exponentials of block-diagonal matrices are also block-diagonal ones, we can obtain the matrix representations of $\exp[\tau K_e/(i\hbar)]$ and $\exp[\tau K_o/(i\hbar)]$ as

$$\exp\left(\frac{\tau K_e}{i\hbar}\right) = \exp\left(\frac{\beta M}{m_1^+}\right) \oplus \exp\left(\frac{\beta M}{m_3^+}\right) \oplus \cdots \oplus \exp\left(\frac{\beta M}{m_{N-1}^+}\right) \tag{21}$$

and

$$\exp\left(\frac{\tau K_o}{i\hbar}\right) = \exp\left(\frac{\beta}{m_1^-}\right) \oplus \exp\left(\frac{\beta M}{m_2^+}\right) \oplus \exp\left(\frac{\beta M}{m_4^+}\right) \oplus \cdots \oplus \exp\left(\frac{\beta M}{m_{N-2}^+}\right) \oplus \exp\left(\frac{\beta}{m_N^+}\right), \tag{22}$$

where we introduce $\beta = -i\tau/(\hbar\alpha)$ for notational simplicity. It is noted that boundary elements denote simple multiplications of scalar numbers in Eq. (22). Explicit expressions of other elements are calculated with the following formula:

$$\exp\left(\frac{\beta M}{m_i}\right) = \frac{1}{2}\begin{pmatrix} 1+e^{2\beta/m_i} & 1-e^{2\beta/m_i} \\ 1-e^{2\beta/m_i} & 1+e^{2\beta/m_i} \end{pmatrix}. \tag{23}$$

Since the coefficient β is an imaginary number, elements of the above matrix are in practice written in terms of trigonometric functions. Consequently, a final expression of the time-evolution matrix due to the kinetic-energy component is obtained by substituting Eqs. (21)–(23) into Eq. (12).

On the other hand, the discretized expression and exponential are easily obtained for $\hat{V}$, because the discretized expression of an interaction potential generally becomes a diagonal matrix. In the following section, the expression of $\hat{V}$ is given after the problems are explicitly defined.

IV. EXAMPLES

In this section, we show calculation results for electrons in AlGaAs QWs as demonstrations of the calculation method developed in Secs. II and III. Preceding the examples, we present definite formulations of the interaction terms for electrons in QWs.

Regarding the z-directional motion of electrons in QWs under a z-polarized oscillating electric field, all states expressed with the same wave function in the z direction can be treated equivalently even if they are labeled with different quantum numbers representing the momentum in the xy directions. Moreover, the optical transitions between two subband states with the same effective mass occur in the same way, no matter where the transitions occur in the momentum space perpendicular to the z direction [20]. Thus, when considering the case that all electrons occupy the same initial state in the z direction, we can ignore the state index for the xy motion and can set

$$\rho(z,t) = N_0|\psi(z,t)|^2, \tag{24}$$

where we can regard N_0 as a sheet electron density in the above interpretation. From the above discussion, the many-electron problem is effectively reduced to a one-electron problem. In the present picture, occupation of higher states due to an external electric field is induced not from the thermal equilibrium but from the nonadiabatic quantum dynamics, noting that electrons are in a pure state with respect to the z direction, whereas they can be in mixed states according to the xy directions.

Using the electron density ρ defined above, the total effective interaction potential in semiconductor QWs is generally described as the following functional:

$$\hat{V}[\rho;z,t] = -\frac{e^2}{\epsilon}\int_{-\infty}^{z} dz'\{[d(z') - \rho(z')](z - z')\} + V^{\mathrm{XC}}[\rho;z] - eV_0(z) - eE_0(z - z_0)\sin\omega t, \tag{25}$$

where e is the charge of an electron, $d(z)$ is the distribution of ionized donors, and $\epsilon(z)$ is a position-dependent effective dielectric constant. In the RHS of Eq. (23), the first two terms compose the effective potential $\hat{V}_{\mathrm{int}}[\rho;z]$, which arises from density-dependent mutual interactions and does not depend explicitly on the time. The former is a Hartree interaction potential, while the latter, $V^{\mathrm{XC}}[\rho;z]$, is an exchange-correlation (XC) potential whose expression is given later. On the other hand, the third and fourth terms are contained in the external potential $\hat{V}_{\mathrm{ext}}(z,t)$; $V_0(z)$ is a fixed and time-independent potential arising from the conduction-band profile and fixed external electric field, while the last term is a time-dependent potential due to an electric field of incident light (electric field amplitude E_0 and angular frequency ω) with z_0 as the origin of the electric potential.

According to the local density approximation in DFT [17,21], the XC potential is given as the following:

$$V^{\mathrm{XC}}[\rho;z] = -\frac{e^4}{32\pi^2\hbar^2}\frac{m(z)}{\epsilon(z)^2}\left(\frac{9\pi}{4}\right)^{1/3}\frac{2}{\pi r_s^*[\rho;z]} \times\left[1 + 0.0545 r_s^*[\rho;z]\ln\left(1 + \frac{11.4}{r_s^*[\rho;z]}\right)\right], \tag{26}$$

which is valid for a wide range of electron densities and is often applied to semiconductor materials. In Eq. (26), the following quantities are introduced:

$$r_s^*[\rho;z] = \left(\frac{3}{4\pi N_0\rho(z)}\right)^{1/3}\frac{1}{a_{\mathrm{B}}^*(z)}, \quad a_{\mathrm{B}}^*(z) = \frac{4\pi\hbar^2\epsilon(z)}{e^2 m(z)}, \tag{27}$$

where the density parameter r_s^* denotes the average distance between electrons scaled by the effective Bohr radius a_{B}^* in the medium.

As mentioned earlier, the total effective interaction potential [Eq. (25)] becomes a real diagonal matrix on the discretized space, i.e.,

$$\mathrm{V}[\rho;t] = \begin{pmatrix} V_1[\rho;t] & 0 & \cdots & 0 \\ 0 & V_2[\rho;t] & 0 & \vdots \\ \vdots & & \ddots & 0 \\ 0 & \cdots & 0 & V_N[\rho;t] \end{pmatrix}, \tag{28}$$

where

$$V_i[\rho;t] = -eV_i^{\mathrm{H}}[\rho] + V_i^{\mathrm{XC}}[\rho] - eV_{0i} - eE_0(i\Delta z - z_0)\sin\omega t, \tag{29}$$

with V_i^{H} as the discretized Hartree potential. The exponential of V becomes a diagonal matrix, whose elements are exponentials of V_i. Further details of the interaction potentials and material parameters in AlGaAs QW are described in Ref. [5].

In the following, we show calculation examples concerning the dynamical properties of electrons in QWs. All results are obtained under the condition of $\Delta z = 0.047$ nm. The time step is chosen as $\Delta t = 0.0002$ fs, which is sufficiently small to suppress numerical errors. A damping potential of a small imaginary value is set around the edges to suppress boundary effects in the practical calculations.

A. Influence of effective-mass mismatch

As the first example, we demonstrate the influence of effective-mass mismatch on the dynamics of an electron in an asymmetric double QW (DQW). Mutual interactions, i.e., Hartree and XC interactions, are omitted to focus our interest only on the effect of effective-mass mismatch.

The time-independent procedure for calculating stationary ground states of QWs in the presence of the effective-mass mismatch is already established [5,6,19]. Thus, we calculate the ground state taking into account the effective-mass mismatch and start the time-evolution calculation from the stationary ground state. The time-evolution calculations are performed in two ways: one is the calculation correctly considering the effective-mass mismatch, and the other is that with a uniform effective mass averaged over the region under consideration. Although the latter treatment is apparently incorrect, the comparison has the meaning of clarifying numerical properties of the present method.

From a physical standpoint, energy and electron distribution must be unchanged during the time evolution in this example. To observe the change of the electron distribution quantitatively, we monitor the average displacement of electrons $[\langle z\rangle = \int dz\, \psi^*(z) z \psi(z)]$ as a benchmark of the distribution. Figures 2(a) and 2(b), respectively, show the average displacement and energy of an electron in an asymmetric DQW as functions of the time. Here, the DQW consists of two GaAs QWs, whose widths are 5.1 and 1.7 nm, separated by a 0.8 nm $Al_{0.44}Ga_{0.56}As$ barrier. Two 17 nm $Al_{0.44}Ga_{0.56}As$ barriers surround the DQW for electron confinement [shown as the inset in Fig. 2(a)]. Here, electron effective masses in GaAs and $Al_{0.44}Ga_{0.56}As$ are $0.067m_e$ and $0.104m_e$, respectively, where m_e denotes the electron mass in vacuum. In Figs. 2(a) and 2(b), we can observe that the electron distribution and energy are conserved in the calculation involving the effective-mass mismatch. Relative numerical errors for energy are less than $10^{-6}$and not observed in the figure.

On the other hand, oscillating behaviors appear in the time-evolution results with averaged effective mass. Calculations were also performed under various numerical conditions: time steps of $\Delta t = 0.0001$, 0.0002, and 0.0005 fs with space intervals of $\Delta z = 0.047$ and 0.071 nm. We observed the same oscillations commonly in these conditions, which means that the oscillation does not originate from a numerical artifact. If we start the averaged mass time-evolution calculations from an stationary initial state obtained without considering the effective-mass mismatch, such oscillations will not be observed. However, this totally uniform-mass calculation produces significant difference between calculation

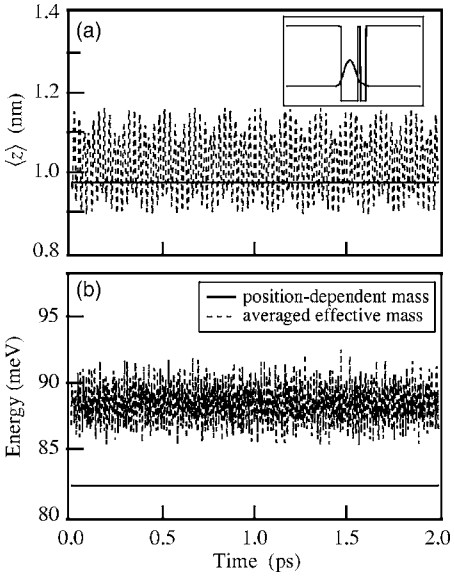

FIG. 2. (a) An average displacement $\langle z \rangle$ and (b) energy of the electron ground state of $GaAs/Al_{0.44}Ga_{0.56}As$ asymmetric DQW as functions of the time. In both figures, solid lines denote the values obtained with taking account of the effective-mass mismatch, while dotted lines denote those obtained with an uniform mass averaged over the position. The QW structure and initial electron distribution are shown as the inset in (a).

results and practically observed phenomena, especially in material systems with larger effective-mass mismatch such as the InAsSb/AlAsSb system. The present method enables correct time-evolution calculations of subband states in semiconductor heterostructures, which calculations have not been available so far.

B. Electron motion after instantaneous turnoff of constant electric field

The second example is the electron oscillation in a uniformly doped single QW (SQW). We start the time-evolution calculation from a stationary initial state under a constant external electric field. When the external electric field is turned off at $t=0$, electrons begin to move to regain an even charge balance, causing the oscillation. Although the instantaneous turnoff of the external electric field cannot be realized in practice, this calculation is a good example of autonomous oscillation in QW.

Figure 3(a) shows the average displacement of electrons in a SQW as a function of time, while Figs. 3(b) and 3(c) illustrate the corresponding spatial distributions of electrons at $t=0$ and 13 fs, respectively. The SQW consists of an 8.5 nm GaAs layer placed between two 17 nm $Al_{0.44}Ga_{0.56}As$ barriers so that electrons are confined even under strong external electric fields. Since the Hartree and XC interactions are considered in this example, electron behavior changes depending on the total number of electrons. For simulating the system containing many electrons in a realistic way, we introduce uniformly distributed donors to give a total sheet electron density of $4.0\times10^{12}/cm^2$. The

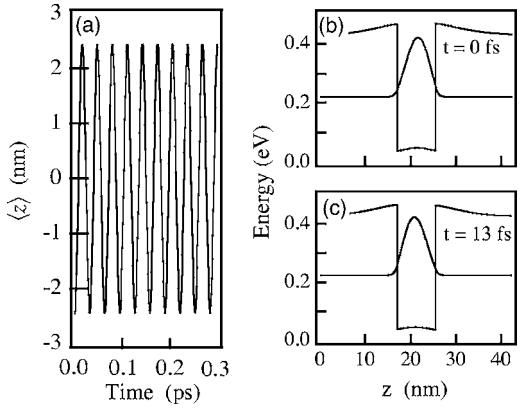

FIG. 3. (a) Temporal oscillation of averaged electron displacement in uniformly doped $GaAs/Al_{0.44}Ga_{0.56}As$ SQW and electron distributions $[|\psi(z)|^2]$ at $t=$(b) 0 and (c) 13 fs. Sheet electron density is $4.0\times10^{12}/cm^2$.

initial state is calculated under an external electric field of 75 kV/cm.

Figure 4 shows a Fourier spectrum of the temporal oscillation in Fig. 3(a), i.e., $|\tilde{z}(\omega)| = |\int dt \langle z(t) \rangle e^{-i\omega t}|$. The main peak at $f(=\omega/2\pi)=31.7$ THz is close to the energy difference between the ground state ($E_0=43.6$ meV from the bottom of the conduction-band edge) and first excited state ($E_1=173.5$ meV) in the absence of nonlinear interactions. Thus we consider that the electron oscillation arises mainly from a quantum beat between the lowest two states. We cannot exactly define the origins of other frequency peaks, but consider the peaks to result from complicated nonlinear effects of the mutual interactions and effective-mass mismatch.

C. Dynamical response of electrons to oscillating external electric fields

One feature of the present method is that we can calculate the nonlinear response of QW states to an external field in the real-time domain. In this section, we provide an example of the electron dynamics under an oscillating electric field with nonlinear interactions. In this example, we consider the same SQW structure that we introduced in the previous example. As mentioned in Sec. IV B, energies of the ground and first excited states are 43.6 and 173.5 meV from the

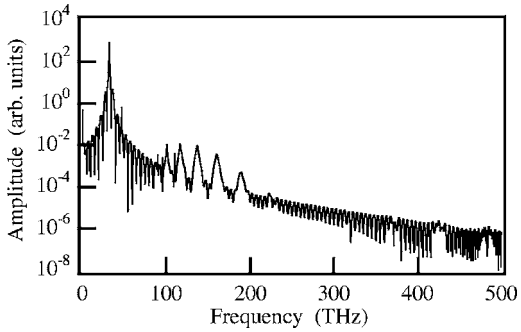

FIG. 4. Fourier spectrum of the temporal oscillation in Fig. 3(a).

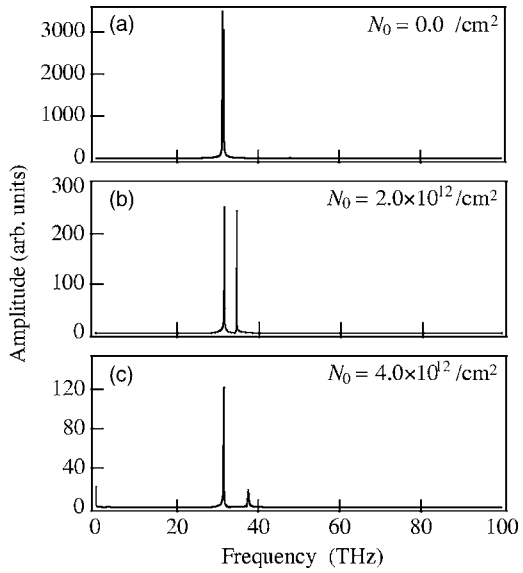

FIG. 5. Fourier spectra of electron oscillation in $GaAs/Al_{0.44}Ga_{0.56}As$ SQW under an oscillating external electric field (f=31.4 THz, $E_0=1.0\times10^5$ V/m). The spectra are obtained similarly as Fig. 4 with charge densities of (a) $N_0=0.0/cm^2$, (b) $2.0\times10^{12}/cm^2$, and (c) $4.0\times10^{12}/cm^2$. Here, $N_0=0.0/cm^2$ denotes the situation without nonlinear interactions.

bottom of the conduction-band edge, respectively, when the nonlinear interactions are absent. Therefore, we can predict that the single QW will absorb electric radiation whose frequency nearly corresponds to the energy difference between the lowest two states (here, 31.4 THz), although a change of the resonant frequency due to nonlinear interactions may exist.

Figures 5(a), 5(b), and 5(c) show Fourier spectra of the electron oscillation under an oscillating external electric field, whose frequency and amplitude are 31.4 THz and 1.0×10^5 V/m, respectively. To study the effects of nonlinear interactions, we compare calculation results with different charge densities: N_0=(a)0.0, (b) 2.0×10^{12}, and (c) $4.0\times10^{12}/cm^2$. As the figures illustrate, a subpeak appears just above the frequency of the external electric field [Fig. 5(b)] and shifts to a higher frequency as the charge density increases [Fig. 5(c)]. This subpeak, we consider, corresponds to the intersubband energy between the lowest two states that suffers from the renormalization effect due to the Hartree and XC interactions. The decrease of the subpeak at higher density is caused by frequency detuning of the external electric field from the resonant frequency of intersubband energy.

In this paper, we showed the Fourier spectra of the average position $\langle z(t)\rangle$ for intuitive demonstration. However, a complex dielectric response is easily obtained as $\tilde{\epsilon}(\omega)=-e\tilde{z}(\omega)/\tilde{E}(\omega)$ (here, the tilde denotes a value in the frequency space) when choosing the origin of $z(t)$ as the weighted average position of positive charges. Thus the present method provides a useful tool for studying nonlinear effects in the dielectric response of QWs.

The *ab initio* TDKS equation will give considerably exact results also for QWs, although it requires a high computational cost because the QW structure must be given as an alignment of atomic potentials in a first-principles calculation. The present method saves on computational cost by applying the effective-mass approximation with complicated nonlinear effects remaining involved. Therefore, the method is the most comprehensive one so far that obeys the effective-mass approximation and has a merit of enabling simulations under realistic situations in a reasonable time. It is also noted that intrasubband relaxation does nothing to the present calculations because the z-directional shape of a wave function is not changed by the intrasubband relaxation. However, incoherent scattering processes, such as scattering due to the roughness of a heterointerface, may cause change to the wave function and damping of the oscillation. By comparing results of the present method with those of the semiconductor Bloch equations [16], we can obtain valuable information that helps to reveal the coherent and incoherent aspects of charge oscillation.

V. SUMMARY AND CONCLUSION

In this paper, we developed an accurate, efficient, and simple method for solving the TDKS equation in semiconductor heterostructures. Applying the space-splitting treatment to the variable-mass kinetic-energy operator in the Hamiltonian, we realized a numerical scheme that can perform time-evolution calculations while involving the effect of effective-mass mismatch at the heterosurface. Interaction-free calculations in an asymmetric DQW showed that the present method involving the effective-mass mismatch in practice conserved the energy and electron distribution with high accuracy. Electron oscillation and nonlinear response of uniformly doped SQWs were also demonstrated. Although the present method cannot treat interband transitions, it does provide a simple and comprehensive picture of intersubband transitions in semiconductor heterostructures under the effective-mass approximation. We expect that the method will be particularly useful for analyzing nonlinear responses of quantum wells under terahertz radiation [22] from the aspect of coherent charge dynamics.

ACKNOWLEDGMENTS

The authors (T.A. and Y.O.) thank T. Hiruma, Y. Suzuki, and Y. Mizobuchi of Hamamatsu Photonics K.K. for their encouragement throughout this work.

APPENDIX: EXPONENTIAL OF KINETIC-ENERGY OPERATOR

In this appendix, we show a direct proof of Eq. (8), although it is easily understood from the Hermiticity of $\hat{K}$.

As mentioned in the text, it is trivial to show that

$$\left((\hat{K}\psi)\frac{\delta}{\delta\psi}-(\hat{K}\psi)^*\frac{\delta}{\delta\psi^*}\right)^k\psi_n=\hat{K}^k\psi_n \tag{A1}$$

for k=1 because $\hat{K}$ does not depend on ψ nor ψ^*. For the second-order relation (k=2),

$$\left((\hat{K}\psi)\frac{\delta}{\delta\psi}-(\hat{K}\psi)^*\frac{\delta}{\delta\psi^*}\right)^2\psi_n=\left((\hat{K}\psi)\frac{\delta}{\delta\psi}-(\hat{K}\psi)^*\frac{\delta}{\delta\psi^*}\right)\hat{K}\psi_n$$
$$=(\hat{K}\psi)\frac{\delta(\hat{K}\psi_n)}{\delta\psi}=(\hat{K}\psi)\frac{\hat{K}\delta\psi_n}{\delta\psi} \tag{A2}$$

is obtained, where the linearity of $\hat{K}$ is considered in the last deformation. To further evaluate Eq. (A2), we consider the following integral:

$$\int_a^b dz'[\hat{K}(z')\psi_m(z')]\hat{K}(z')\delta\psi_n$$
$$=-\frac{\hbar^2}{2}\int_a^b dz'[\hat{K}(z')\psi_m(z')]\frac{\partial}{\partial z'}\frac{1}{m(z')}\frac{\partial}{\partial z'}\delta\psi_n, \tag{A3}$$

where $\delta\psi_n$ denotes a variation of the wave function $\psi_n(z)$. In this appendix, the dependence of $\psi_n(z)$ on the time variable is dropped for notational simplicity. Applying the partial integral formula to the RHS of Eq. (A3) and ignoring surface terms, we obtain

$$\int_a^b dz'[\hat{K}(z')\psi_m(z')]\frac{\partial}{\partial z'}\frac{1}{m(z')}\frac{\partial}{\partial z'}\delta\psi_n$$
$$=\left[\hat{K}(z')\psi_m(z')\right]\frac{1}{m(z')}\frac{\partial}{\partial z'}\delta\psi_n\Bigg|_a^b$$
$$-\int_a^b dz'\left(\frac{\partial}{\partial z'}\hat{K}(z')\psi_m(z')\right)\frac{1}{m(z')}\frac{\partial}{\partial z'}\delta\psi_n$$
$$=-\int_a^b dz'\left(\frac{1}{m(z')}\frac{\partial}{\partial z'}\hat{K}(z')\psi_m(z')\right)\frac{\partial}{\partial z'}\delta\psi_n.$$

Repeating the similar operation again, the above equation is further modified as

$$-\left(\frac{\partial}{\partial z'}\frac{1}{m(z')}\frac{\partial}{\partial z'}\hat{K}(z')\psi_m(z')\right)\delta\psi_n\Bigg|_a^b$$
$$+\int_a^b dz'\left(\frac{\partial}{\partial z'}\frac{1}{m(z')}\frac{\partial}{\partial z'}\hat{K}(z')\psi_m(z')\right)\delta\psi_n$$
$$=-\frac{2}{\hbar^2}\int_a^b dz'[\hat{K}^2(z')\psi_m(z')]\delta\psi_n. \tag{A4}$$

From Eqs. (A3) and (A4), the following formula is derived:

$$\int_a^b dz'[\hat{K}(z')\psi_m(z')]\hat{K}(z')\delta\psi_n=\int_a^b dz'[\hat{K}^2(z')\psi_m(z')]\delta\psi_n. \tag{A5}$$

Here, with the help of Eq. (6) in the text and using Eq. (A5), we obtain the following relation:

$$(\hat{K}\psi)\frac{\hat{K}\delta\psi_n}{\delta\psi}=\sum_{m=1}^{N_0}\int_a^b dz'[\hat{K}(z')\psi_m(z')]\hat{K}(z')\frac{\partial\psi_n}{\partial\psi_m(z')}$$
$$=\sum_{m=1}^{N_0}\int_a^b dz'[\hat{K}^2(z')\psi_m(z')]\frac{\partial\psi_n}{\partial\psi_m(z')}$$
$$=\hat{K}^2\psi_n. \tag{A6}$$

Thus, substituting Eq. (A6) into Eq. (A2), we can prove Eq. (A1) for $k=2$. By repeating the above derivation, Eq. (A1) is shown to be correct for general k. Finally, the following formula is obtained:

$$\exp\left[\alpha\left((\hat{K}\psi)\frac{\delta}{\delta\psi}-(\hat{K}\psi)^*\frac{\delta}{\delta\psi^*}\right)\right]\psi_n$$
$$=\sum_{k=0}^{\infty}\frac{\alpha^k}{k!}\left((\hat{K}\psi)\frac{\delta}{\delta\psi}-(\hat{K}\psi)^*\frac{\delta}{\delta\psi^*}\right)\psi_n$$
$$=\sum_{k=0}^{\infty}\frac{\alpha^k}{k!}\hat{K}^k\psi_n$$
$$=\exp(\alpha\hat{K})\psi_n. \tag{A7}$$

[1] T. Ando, Phys. Rev. B **13**, 3468 (1976).
[2] G. E. W. Bauer and T. Ando, Phys. Rev. B **34**, 1300 (1986).
[3] W. L. Bloss, J. Appl. Phys. **66**, 3639 (1989).
[4] M. Seto and M. Helm, Appl. Phys. Lett. **60**, 859 (1992).
[5] T. Ando, H. Taniyama, N. Ohtani, M. Nakayama, and M. Hosoda, J. Appl. Phys. **94**, 4489 (2003).
[6] T. Ando, M. Nakayama, and M. Hosoda, Phys. Rev. B **69**, 165316 (2004).
[7] P. Hawrylak, Phys. Rev. B **39**, 6264 (1989).
[8] For a review, T. L. Beck, Rev. Mod. Phys. **72**, 1041 (2000); G. Onida, L. Reining, and A. Rubio, *ibid.* **74**, 601 (2002), and references therein.
[9] G. Bastard, Phys. Rev. B **24**, 5693 (1981).
[10] I. Galbraith and G. Duggan, Phys. Rev. B **38**, 10057 (1988).
[11] G. T. Einevoll and L. J. Sham, Phys. Rev. B **49**, 10533 (1994).
[12] N. Watanabe and M. Tsukada, Phys. Rev. E **65**, 036705 (2002).
[13] J. L. Richardson, Comput. Phys. Commun. **63**, 84 (1991).
[14] H. De Raedt and K. Michielsen, Comput. Phys. **8**, 600 (1994).
[15] T. Ando and M. Fujimoto, Phys. Rev. E **72**, 026706 (2005).
[16] For example, H. Haug and S. W. Koch, *Quantum Theory of the Optical and Electric Properties of Semiconductors*, 4th ed. (World Scientific, Singapore, 2004).
[17] See, for a review, M. C. Payne, M. P. Teter, D. C. Allan, T. A. Arias, and J. D. Joannopoulos, Rev. Mod. Phys. **64**, 1045 (1992) and references therein.
[18] M. Suzuki, Phys. Lett. A **146**, 319 (1990).
[19] T. Ando, H. Taniyama, N. Ohtani, M. Hosoda, and M. Na-

kayama, IEEE J. Quantum Electron. **38**, 1372 (2002).
[20] This picture fails for an interband transition because the energy required for the interband transition depends on where the transition occurs in the momentum space.
[21] O. Gunnarsson and B. I. Lundqvist, Phys. Rev. B **13**, 4274 (1976).
[22] F. Rossi and T. Kuhn, Rev. Mod. Phys. **74**, 895 (2002), and references therein.